Hydride as a Leaving Group in Nucleophilic Aromatic Substitution

Stanislav Melnikov[1], Donghun Hwang[2,3], Bohyun Park[2,3], Martin Lutz[4], Mu-Hyun Baik*[3,2], Daniël L.J. Broere*[1]

[1]Organic Chemistry and Catalysis, Institute for Sustainable and Circular Chemistry, Faculty of Science, Utrecht University, Universiteitsweg 99, 3584 CG Utrecht, The Netherlands

Email: d.l.j.broere@uu.nl

[2]Department of Chemistry, Korea Advanced Institute of Science and Technology (KAIST), Daejeon 34141, Republic of Korea

[3]Centre for Catalytic Hydrocarbon Functionalizations, Institute for Basic Science (IBS), Daejeon 34141, Republic of Korea

Email: mbaik2805@kaist.ac.kr

[4]Structural Biochemistry, Bijvoet Centre for Biomolecular Research, Faculty of Science, Utrecht University Universiteitsweg 99, Utrecht, The Netherlands

ABSTRACT: The direct functionalisation of unactivated hydrocarbons remains one of the major challenges in modern chemistry. Here we demonstrate that a simple ruthenium complex with a chelating $^{t\text{Bu}}$PN ligand can mediate the nucleophilic aromatic substitution of hydrogen (S_NArH) in benzene. Key intermediates were kinetically trapped in low-temperature NMR experiments, providing important insights into the reaction mechanism which is further supported with in-depth DFT studies. These data show that the substitution occurs via an unprecedented mechanism that involves the rear-side nucleophilic addition of the exogenous nucleophile to the ruthenium-bound benzene followed by an intramolecular hydride migration that is facilitated by deprotonation of $^{t\text{Bu}}$PN ligand. The broad range of nucleophiles amenable to this reaction, including classical non-nucleophilic bases, showcases the versatility of this reaction and makes it a promising candidate for further developments in the area of S_NArH.

Introduction

Electrophilic aromatic substitution (S_EAr) is one of the oldest reactions known for functionalisation of aromatic molecules.[1,2] Its counterpart, nucleophilic aromatic substitution (S_NAr) is historically less used notwithstanding the ability to access structures that lie outside of the scope of S_EAr. Even though S_NAr can be considered as a 'mirror reflection' of S_EAr polarity-wise, arenes are less reactive towards exogeneous nucleophiles.[3–5] The most widely used strategy for activating benzene derivatives towards S_NAr lies in incorporation of electron-withdrawing groups (EWGs). These decrease the electron density on the aromatic ring facilitating nucleophilic addition at the position that features a leaving group, such as F or Cl, to give a σ^X-adduct (the so-called Jackson–Meisenheimer complex, Fig. 1a). The anionic σ^X-adduct is generally unstable and readily loses the leaving group, thereby restoring aromaticity.[6,7] Given that the leaving group eliminates in an anionic form, nucleophilic aromatic substitution of hydrogen (S_NArH) is more challenging. However, there have been reports that it can be formally realised in two steps through a separate oxidation of the pre-formed σ^H-adduct (Fig.1b).[8,9]

An alternative method of activating aromatic molecules towards nucleophilic addition involves their coordination to a transition metal complex. Such reactions have been explored extensively (mostly for such metals as Cr and Ru),[10–21] resulting in the formation of stable cyclohexadienyl complexes, which can be seen as a transition metal stabilised analogues of the σ^X-adducts. Although this reactivity avoids installation of EWGs on the aromatic ring and has been used to mediate S_NAr reactions even in complex molecules, the arene still requires a conventional leaving group to mediate the substitution reactions.[13,22–24] Similar to the metal-free reaction, a subsequent oxidation step of the transition metal stabilised Jackson–Meisenheimer complex has been demonstrated to mediate formal S_NArH for simple arenes (Fig.1c).[10,13,25–28]. Theoretically, an intramolecular hydride migration from the cyclohexadienyl-anion to the bound metal centre would allow for H to serve as a leaving group in a S_NArH reaction (Fig. 1e). However, such reactivity has not been reported to date.

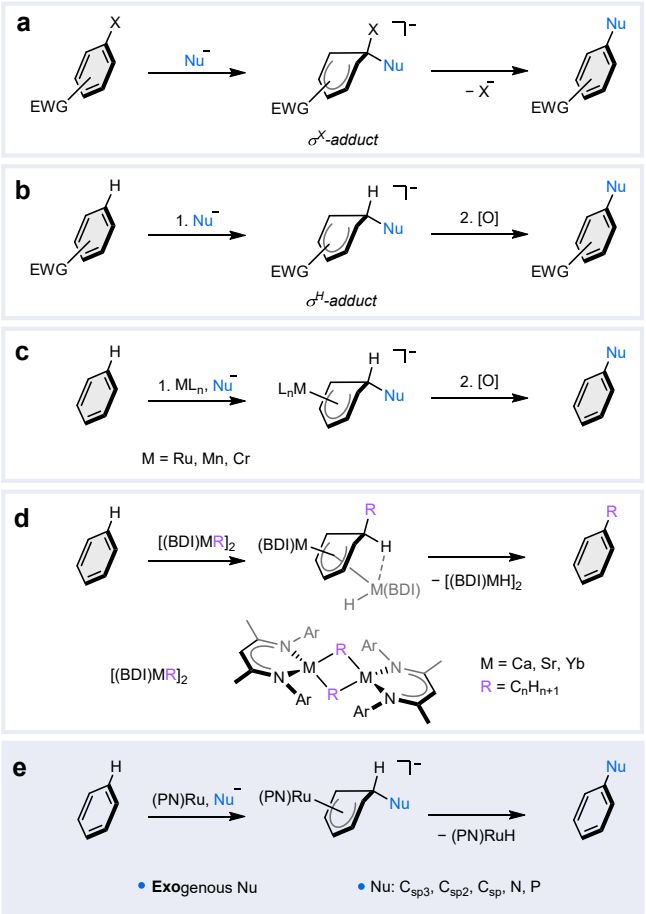

Fig. 1. Strategies for nucleophilic aromatic substitution. a, S_NAr in electron-deficient arenes where X is a leaving group. **b**, Addition of nucleophiles observed in electron-deficient arenes leads to the formation of Jackson–Meisenheimer complexes that require an additional step of oxidation for the formal S_NArH to occur. **c**, Nucleophilic addition in transition metal arene complexes. If the arene does not have good leaving groups, a subsequent oxidation of the metal-stabilised Jackson–Meisenheimer adduct is necessary to mediate formal S_NArH. **d**, Metal-mediated S_NArH alkylation of benzene with β-diketiminate (BDI) complexes of Ca,[29] Sr[30] and Yb[31] which employ *endogenous* nucleophiles; no oxidation step is required. **e**, This work: Metal-mediated S_NArH in benzene with a readily accessible $^{t\text{Bu}}$PN-Ru complex and various types of *exogenous* nucleophiles (including very bulky ones); no oxidation step is required.

The feasibility of such a pathway is supported by an analogous intermolecular process, reported by Hill, Maron and co-workers in 2017 (Fig.1d),[29] which enables the nucleophilic alkylation of benzene using β-diketiminate (BDI) supported Ca alkyl complexes. Subsequent works[30,31] showed that this reaction can also be performed using similar strontium- and ytterbium-based complexes. Recent computational studies[32] suggest that the reaction with the Ca and Sr complexes happens via a front-side nucleophilic addition of the *endogenous* carbanion to the metal-coordinated arene. Subsequently, a rear-side hydride abstraction is facilitated by another calcium complex in an intermolecular fashion. Despite this process enabling oxidant-free S_NArH, it has thus far only been shown for alkylation as the reaction is limited by the stabilisation of a potent 'intramolecular nucleophile' that is bound to the BDI complex. Hence, it remains unknown whether it would be viable to utilise other types of nucleophiles in metal-mediated S_NArH reactions.

Herein, we describe a new pathway that enables nucleophilic aromatic substitution in benzene using *exogenous* nucleophiles and wherein hydride serves as the leaving group (Fig.1e). This peculiar reactivity is made possible by a simple ruthenium complex, which both activates the arene towards nucleophilic attack and mediates an unprecedented intramolecular hydride transfer to complete the S_NArH reaction. We demonstrate the versatility of this reaction, highlighting its applicability with a diverse range of nucleophiles, including those that are commonly considered as non-nucleophilic bases. Moreover, in this Article we detail a thorough investigation involving isotopic labelling, kinetic trapping of key intermediates and extensive computational studies, which elucidates the mechanism of this unusual reaction.

Results and discussion

Synthesis and characterisation

While exploring Milstein-like aromatisation-dearomatisation cooperativity[33] with complex [($^{t\text{Bu}}$PN)RuCl(C_6H_6)]PF_6 (**1**), we serendipitously found that the addition of 1 equiv $KN(TMS)_2$ to **1** in THF at room temperature yields a dark brown mixture of two inseparable species with the ratio 70:30 (Fig. 2a). Analysis of the solution ^{1}H nuclear magnetic resonance (NMR) spectra in THF-d_8 showed that the main species featured all the characteristic resonances of the expected deprotonated compound [($^{t\text{Bu}}$PN*)RuCl(C_6H_6)K(THF)$_n$]PF_6 (**2-K**) (See Supplementary Section S1.2 for characterisation). Surprisingly, the second species featured a doublet at δ = –7.77 ppm and two doublets of doublets at d = 3.63 and 3.26 ppm that all integrate equally. This indicated the presence of a hydride and a non-deprotonated form of the $^{t\text{Bu}}$PN ligand featuring diastereotopic methylene hydrogens, respectively. Additionally, this new species did not contain a coordinated benzene molecule; instead five separated multiplets were found in the ^{1}H spectrum in the range from δ = 6.27 to 4.64 ppm. Based on the spectroscopic data we assign this species to [($^{t\text{Bu}}$PN)RuH(PhN$(TMS)_2$)]PF_6 (**3**, Fig. 2a). Intrigued by the formation of this unusual species, which we hypothesised as the product of S_NArH at the coordinated benzene, we decided to look into this surprising reactivity in more detail.

The addition of complex **1** to 2 equiv of $KN(TMS)_2$ in THF at room temperature leads to an instant colour change from yellow to brown, concomitantly with the formation of ($^{t\text{Bu}}$PN*)RuH(PhN$(TMS)_2$) (**4**), which was isolated in 97% yield (Fig. 2a). The ^{1}H NMR spectrum of **4** in C_6D_6 shows a doublet at δ = –7.76 ppm and a doublet at δ = 3.49 ppm, both of which integrate equally, and are characteristic of a hydride and a methine linker of a dearomatized $^{t\text{Bu}}$PN ligand ($^{t\text{Bu}}$PN*), respectively. Similar to **3**, the ^{1}H NMR spectrum also features five magnetically coupled multiplets (all integrating to 1H) spread within δ = 5.11 and 4.14 ppm and a large singlet at 0.25 ppm, which integrates to 18H. From this data we concluded that complex **4** is the deprotonated analogue of **3**. This is supported by the X-ray crystal structure determination (Fig.

2b, Supplementary Section S6.2) of brown single crystals of **4** obtained from a concentrated pentane solution at –40 °C.

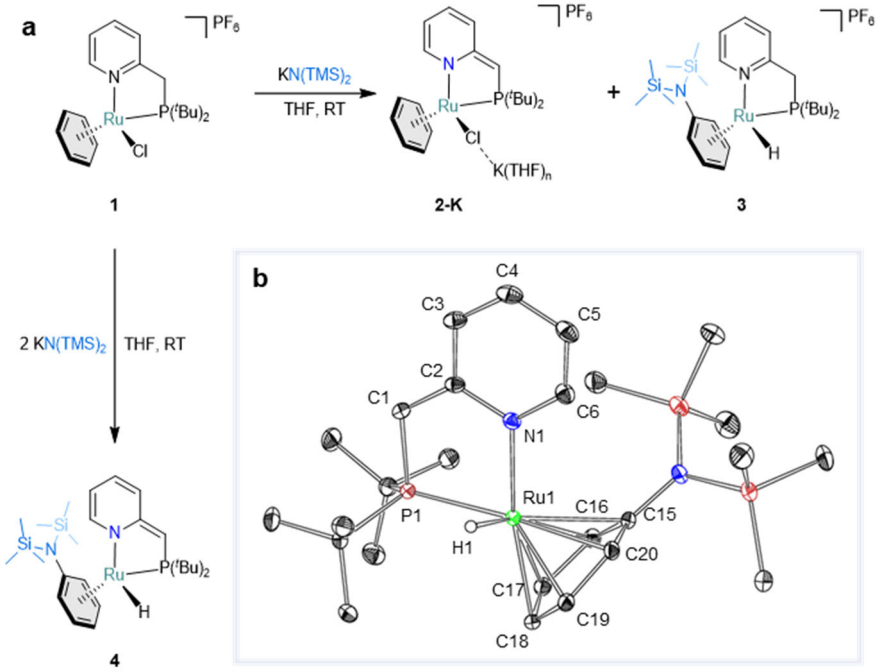

Fig. 2. Substitution of a hydride at a coordinated benzene with KN(TMS)$_2$. a, The reaction between **1** and KN(TMS)$_2$. The addition of 1 equiv of the base leads to the mixture of **2-K** and **3** (70:30), whereas 2 equiv yield compound **4**. **b**, Solid-state molecular structure of **4** (ellipsoids drawn at the 30% probability level). The hydrogen atoms except for the hydride are omitted for clarity. Selected bonds (Å) and angles (°): Ru(1)-PhN(TMS)$_2^{centroid}$ = 1.7821(7), Ru(1)-N(1) = 2.0961(11), Ru(1)-P(1) = 2.3325(3), Ru(1)-C(15) = 2.4275(13), Ru(1)-C(16) = 2.3775(14), Ru(1)-C(17) = 2.2091(14), Ru(1)-C(18) = 2.2055(14), Ru(1)-C(19) = 2.1776(14), Ru(1)-C(20) = 2.2409(13), C(1)-C(2) =1.382(2), C(2)-N(1) = 1.3910(18), C(2)-C(3) = 1.4415(19), C(3)-C(4) = 1.359(2), C(4)-C(5) = 1.407(2), C(5)-C(6) = 1.370(2), N(1)-C(6) = 1.3555(18), N(1)-Ru(1)-P(1) = 81.75(3), N(1)-Ru(1)-PhN(TMS)$_2^{centroid}$ = 131.28(4), P(1)-Ru(1)-PhN(TMS)$_2^{centroid}$ = 140.17(3).

The solid-state structure of **4** revealed a piano stool type complex in which ruthenium is bound to both the arene ring as well as the $^{t\text{Bu}}$PN* ligand. The found interatomic distances in the $^{t\text{Bu}}$PN* ligand are characteristic of a dearomatised pyridine ring and a deprotonated methylene linker (Fig. 2b), in agreement with the NMR data. This anionic binding mode of the bidentate ligand enforces the small N(1)-C(2)-C(1)-P(1) dihedral angle of 2.10(19)°. The hydride ligand was located in difference Fourier maps and was refined freely. In addition, the molecular structure shows a η^6-coordinated silylated aniline, which is consistent with the NMR data. The coordination sphere of the metal centre is best described as a distorted piano-stool geometry with a very long Ru-Aniline^{centroid} distance of 1.7821(7) Å (only 4% of reported η^6-arene Ru structures have this distance longer according to the Cambridge Structural Database,[34] see Supplementary Figs. S82-84). The ruthenium is bound unevenly to all the carbons of the aniline moiety, and a slight ring slippage is observed away from the N(TMS)$_2$ side with respect to the coordinated metal (0.194 Å). It is noticeable that the Ru-C bonds are clustered to two groups. Two of the bonds are longer compared to the other four (Ru-C = 2.3775(14) – 2.4275(13) Å for C(15)-C(16) *vs* Ru-C = 2.1776(14) – 2.2409(13) Å for C(17)-C(20), see Supplementary Tables S6-7). This type of arene coordination can be also considered as 'η^4+η^2' and is associated with the *trans*-effect of the tertiary phosphine[35,36]

as well as steric repulsion emerged between PhN(TMS)$_2$ fragment and $^{t\text{Bu}}$PN* ligand. This explains the relatively large separation of the aromatic aniline resonances in the ^{1}H NMR spectrum.

Mechanistic investigations

The reactivity observed for complex **1** is remarkable since KN(TMS)$_2$ is considered a non-nucleophilic base while benzene is typically inert to S_NAr. Intrigued by this atypical reactivity, we set out to elucidate the mechanism underlying this reaction. To ascertain the origin of the hydride in **4**, we synthesised an isotopically labelled analogue, **4-D** (Fig. 3). For that, benzene-d_6 was reduced with lithium metal and ethylenediamine in Et$_2$O/EtOD according to a modified Birch-like procedure,[37] which gave a mixture of partially deuterated cyclohexadienes. A subsequent reaction with ruthenium trichloride gave partially deuterated Ru_2Cl_4(benzene)$_2$ (**5**), which was used to synthesise **1-D** with 61% deuteration of the coordinated benzene. Reacting **1-D** with two equiv of KN(TMS)$_2$ yielded compound **4-D** with 57% and 56% deuteration for the coordinated aniline and hydride, respectively. The relative integration of the signals in ^{1}H NMR spectra of compound **4-D** shows an equal degree of deuteration between the hydridic and aromatic resonances, confirming that the hydride originates from the benzene (Supplementary Figs. S14-18). It is noteworthy, that no H/D scrambling with the $^{t\text{Bu}}$PN ligand was observed in the product, excluding arene C-H bond activation via metal-ligand cooperation.[38,39]

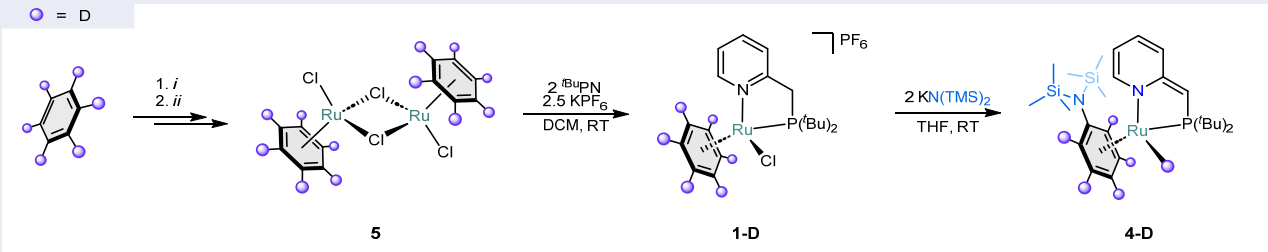

Fig. 3. Isotopic labelling experiments. Synthetic route towards compound **4-D**. The purple balls represent the positions where significant amount of deuterium was detected in ^{1}H qNMR. The reactions conditions: *i*) Li metal, ethylenediamine, EtOD in THF at 0 °C; *ii*) $RuCl_3 \cdot xH_2O$ in EtOD (reflux). For more details see Supplementary Section S1.1.

Based on the isotopic labelling experiments two plausible mechanistic pathways were hypothesised for the substitution reaction: i) deprotonation of $^{t\text{Bu}}$PN with subsequent aromatic substitution of the hydride (Fig. 4a *top*) and ii) aromatic substitution followed by deprotonation of the ligand (Fig. 4a *bottom*). To shed light on the operational mechanism, a series of NMR experiments was conducted involving the reaction between **1** and KN(TMS)$_2$. After the addition of only 1 equiv of KN(TMS)$_2$ to **1** at –78 °C in THF-d_8, ^{1}H NMR analysis at –60 °C showed conversion to a single major species that neither contained a hydride, nor a symmetrical benzene. The proton signals corresponding to the former aromatic ring of the benzene were found as six equally integrating multiplets in a wide range of δ = 5.10 to 2.76 ppm. Based on the data obtained through a combination of ^{1}H-^{1}H TOCSY & ^{1}H-^{31}P HMBC analysis, we assign this compound as intermediate **Int1** (Fig. 4b, Supplementary Figs. S31-36), which contains a η^5-cyclohexadienyl ligand formed by nucleophilic addition of N(TMS)$_2^-$ to the coordinated benzene, resembling the Jackson–Meisenheimer complex. The extremely upfield-shifted proton signal at δ = 2.76 ppm corresponds to the allylic proton of the cyclohexadienyl fragment. Surprisingly, the methylene linker of the complex is intact despite the addition of such a potent base as KN(TMS)$_2$. Slow warming up of the reaction mixture to RT showed partial decomposition of **Int1,** giving a mixture of species that converted mostly to complex **2-K** after 16 hours at RT (Supplementary Fig. S37). This shows that

the nucleophilic addition that forms **Int1** is a kinetically-driven process contrarily to the deprotonation of the ligand that leads to **2-K**, which is a more thermodynamically favourable pathway. Moreover, it also shows that the nucleophilic addition is reversible (Fig. 4b). The formation of **3** in the initial reaction of **1** with 1 equiv of $KN(TMS)_2$ (Fig. 2a) is ascribed to the higher basicity of **4** compared to **2-K** (See Supplementary Section S1.2).

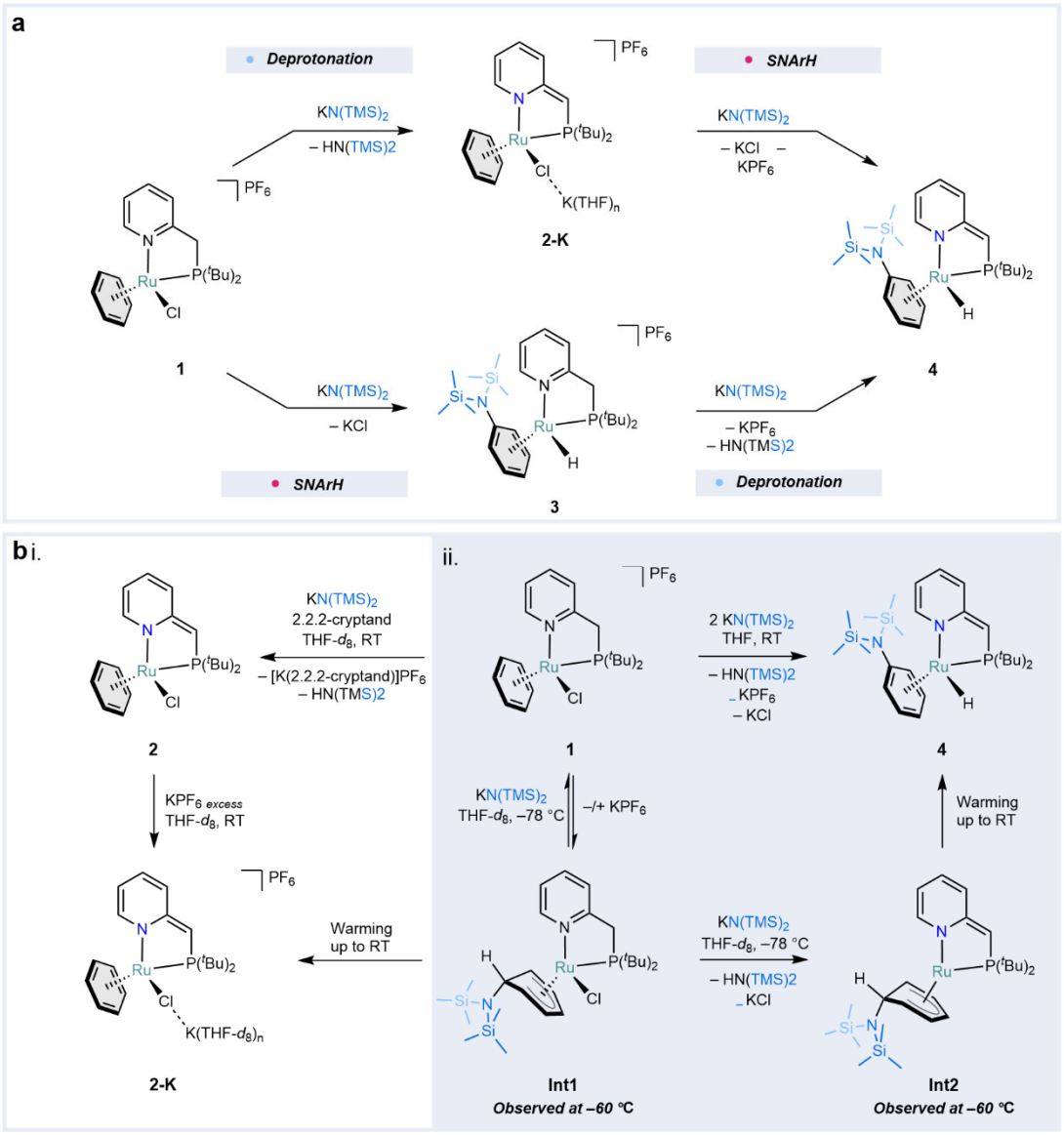

Fig. 4. Plausible mechanisms and mechanistic investigations of the S_NArH reaction with $KN(TMS)_2$. a, Plausible mechanistic pathway involving first deprotonation of the methylene linker of the $^{t\text{Bu}}$PN ligand followed by nucleophilic aromatic substitution of a hydride (*top* path) and a pathway wherein the S_NArH precedes the deprotonation of the $^{t\text{Bu}}$PN ligand (*bottom* path). **b**, Mechanistic NMR experiments at RT (i) and –60 °C (ii) featuring the structures of two kinetically-trapped metal-stabilised Jackson–Meisenheimer intermediates **Int1** and **Int2**.

^{1}H NMR analysis at –60 °C of a mixture resulting from the addition of 2 equiv of $KN(TMS)_2$ to **1** in THF-d_8 at –78 °C allowed us to observe a new species **Int2**. Similar to the analogous experiment with 1 equiv of $KN(TMS)_2$ that gave **Int1**, no resonances in the hydridic region were detected and seven equally integrating resonances within δ = 5.28 and 3.10 ppm were found. Together with ^{1}H-^{31}P HMBC analysis, a broad signal at δ = 3.25 ppm was assigned as a methine proton suggesting

deprotonation of the $^{t\text{Bu}}$PN ligand (Fig. 4b, Supplementary Figs. S38-43). The other six signals were magnetically coupled as shown by ^{1}H-^{1}H TOCSY NMR analysis and were assigned as η^5-cyclohexadienyl protons. From this data we conclude that compound **Int2** is another metal-stabilised Jackson-Meisenheimer intermediate, which forms upon deprotonation of **Int1**. Warming up the reaction mixture to RT resulted in a clean formation of compound **4** already at –20 °C supporting our findings regarding the nature of **Int2** (Supplementary Figs. S44-47). The fact that compound **4** forms cleanly only upon warming up demonstrates that the hydride migration is the rate-determining step of the reaction.

Computational studies

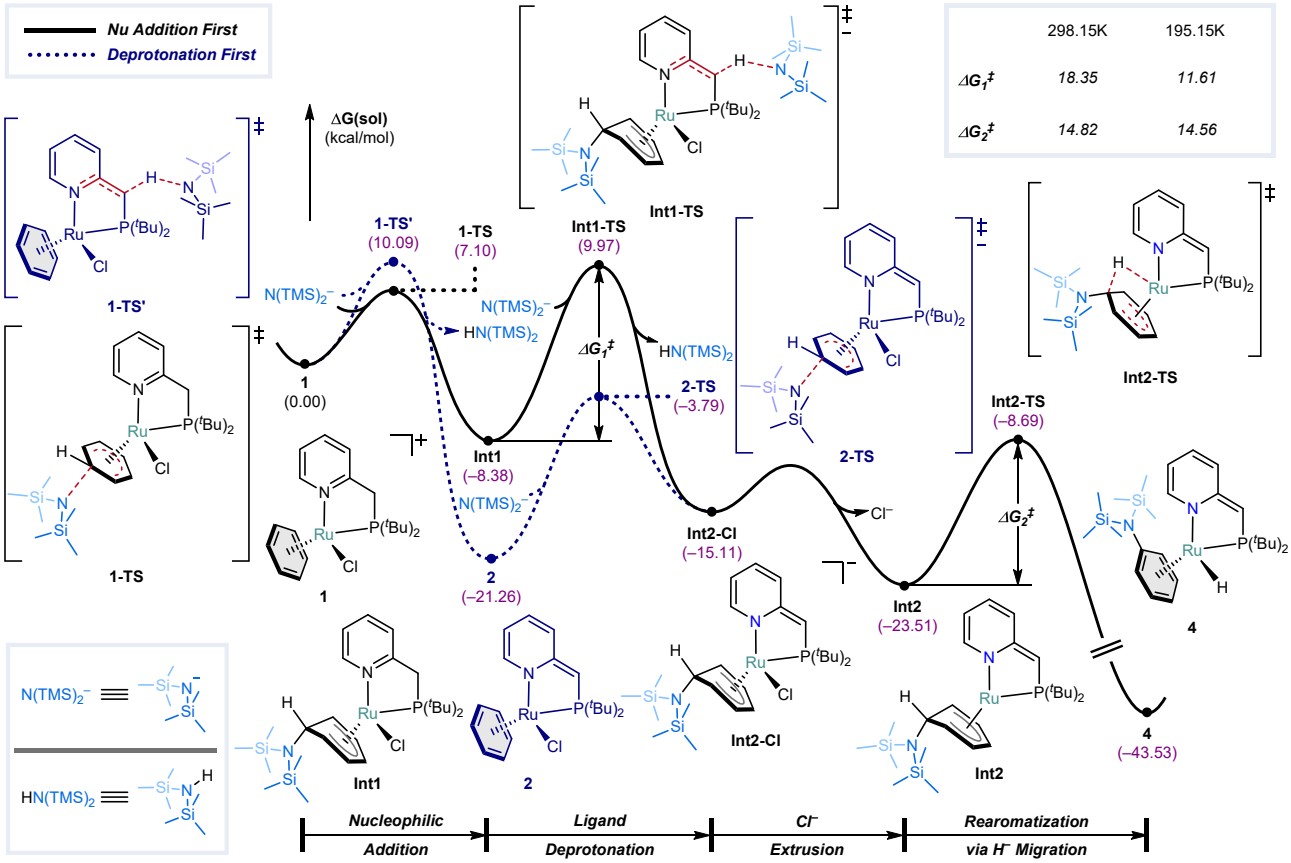

Fig. 5. Computed reaction profile of the S_NArH mediated by complex 1. Only the most facile pathway is shown. For details and other calculated energy profiles see Supplementary Section S3.1.

To gain a deeper understanding of the mechanism of the S_NArH reaction, density functional theory (DFT) calculations were performed at the B3LYP-D3(BJ)/def2-TZVPD/def2-ECP(Ru)//B3LYP-D3(BJ)/def2-SVP/def2-ECP(Ru) level of theory using the ORCA 5.0.3 software (See Methods for details). Given the difficulty and potential errors of modelling solvated structure of complex associated with K^+ and THF,[40] bis(trimethylsilyl)amide anion without its cationic partner was utilised to model the entire reaction. Both mechanistic scenarios (Fig. 4a) were thoroughly analysed – where direct nucleophilic addition to **1** (**1-TS**, Fig. 5) happens first or the ligand deprotonation (**1-TS'**, See Supplementary Section S3 for more detail). The calculations revealed that the formation of metal-stabilised Jackson-Meisenheimer complex **Int1** via **1-TS**, featuring a barrier of 7.1 kcal/mol, is kinetically more facile than the formation of deprotonated complex **2** via **1-TS'**, which is consistent with the experimental results. An additional equivalent

of $KN(TMS)_2$ deprotonates a methylene proton on the ligand from **Int1** with a step barrier of 18.4 kcal/mol, yielding intermediate **Int2-Cl**. This deprotonation enhances the electron-donating ability of the nitrogen in the pyridine moiety due to the dearomatisation of the ligand, rendering the metal centre more electron-rich. In addition to this, the anionic nature of the complex in **Int2-Cl** propels the extrusion of Cl^-, compared to an intermediate where the extrusion would occur without the deprotonation event, even though this change in electronic property of the ruthenium centre increases the barrier of the hydride migration (for the profile see Supplementary Fig. S54). Chloride extrusion generates the vacant site on the metal centre required for the final intramolecular hydride migration with a step barrier of 14.5 kcal/mol, completing the S_NArH on benzene. Notably, based on the reaction profile, the deprotonation step is expected to have the highest barrier within the reaction at room temperature, however, the hydride migration is estimated to have the highest barrier at the low temperature, consistent with observations from NMR experiments. Given that the deprotonation step is a bimolecular process and the hydride migration occurs within a single molecule, the dramatic alternation in the energies is a direct consequence of the diminished entropic penalty resulting from the temperature decrease. This alternation makes the final hydride migration be the rate determining step of the reaction and enables to see intermediate **Int2**. These calculation results strongly align with the observation of **Int2** at low temperature, and the formation of **4** when the reaction mixture is allowed to warm up.

Scope of the reaction

The state-of-the-art S_NArH reactions using β-diketiminate complexes (Fig. 1d) are limited to intramolecular alkyl nucleophiles. Given that the reactivity described above involves an exogenous nucleophile that is commonly used as a non-nucleophilic bulky base, we investigated the scope of nucleophiles amenable to the Ru-mediated S_NArH reaction. Motivated by both obtaining the metal-free substitution product and the difficulties to accurately determine spectroscopic yields with some nucleophiles used, we first investigated the conditions that enable liberation of the aniline in **4** (Supplementary Section S4.1). Although it is known that the arene exchange reactions on Ru are challenging, especially in neutral complexes featuring electron-rich arenes,[41,42] we found that irradiation of a benzene solution of **4** with a 365 nm UV light enables partial arene exchange to give "free" $PhN(TMS)_2$ in a modest yield of 40% based on GC analysis (**VI**, Fig. 6). This suggests the presence of the strong binding energy between the ruthenium centre and bis-silylated aniline (See Supplementary Section S3.3 for TD-DFT calculations). Although it is not optimal, we used this protocol to assess the scope of nucleophiles amenable to the S_NArH reaction in **1**. GC analysis of the reaction mixtures (after arene exchange) with $C(sp^3)$-based nucleophiles *n*-butyl lithium (^{n}BuLi) and benzyl potassium (BnK) showed the formation of the targeted butyl benzene (**I**) in 9% yield and diphenyl methane (**II**) in 31% yield. Similarly, a reaction with phenylmagnesium bromide as a $C(sp^2)$-based nucleophile showed formation of biphenyl (**III**) in 35 % yield. A reaction with vinyl magnesium bromide to give styrene (**IV**) is not compatible with our protocol given that the reaction product polymerises under UV light.[43] However, ^{1}H NMR analysis of the reaction mixture after mixing **1** and vinyl magnesium bromide showed 21 % formation of two hydride species at similar chemical shifts as those observed for complex **4** (Supplementary Figs. S60-61). This suggests the formation of a similar complex with coordinated styrene instead. Using different arene exchange protocols, triphenylphosphine (**VI**) and diphenyl acetylene (**VII**) were generated by reaction with potassium diphenyl phosphide or lithium phenyl acetylide, respectively, albeit in poor yields. Although these non-optimised yields and protocols are far from practical, it demonstrates that the Ru-mediated S_NArH reaction is compatible with a variety of nucleophiles.

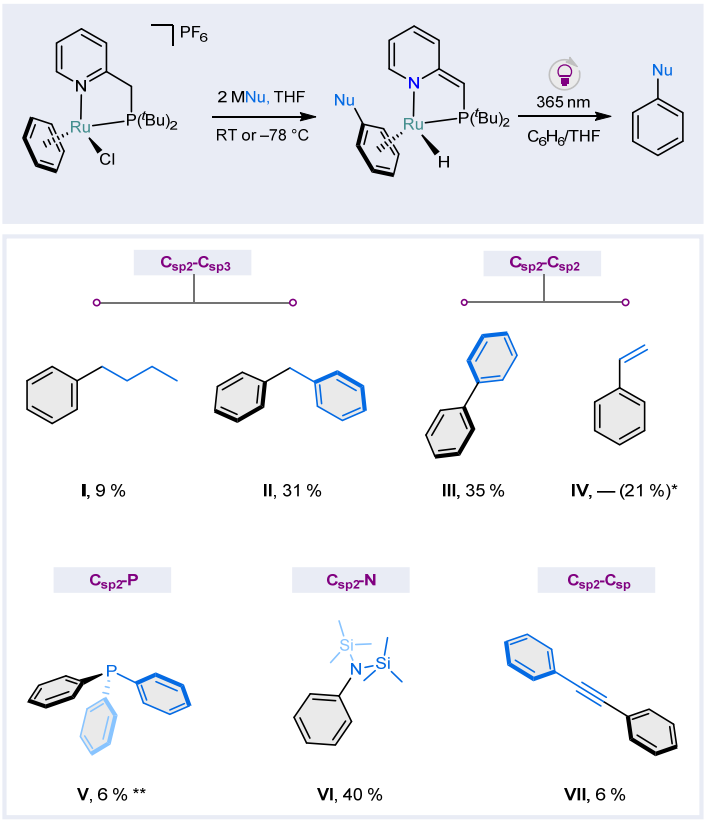

Fig. 6. S_NArH on benzene mediated by complex 1 with diverse nucleophile. I: *n*-butyllithium, **II**: benzyl potassium, **III**: phenylmagnesium bromide, **IV**: vinyl magnesium bromide (quantified based on the qNMR data of the corresponding complex), **V**: potassium diphenylphosphide (analysed in the form of its oxide), **VI**: potassium bis(trimethylsilyl)amide, **VII**: lithium phenyl acetylide (basic work-up was done instead of the UV irradiation). The yields were determined by GC analysis. For more details see Supplementary Section S4.2.

In conclusion, we uncovered a new Ru-mediated mechanistic pathway that enables the nucleophilic aromatic substitution of hydrogen (S_NArH) on benzene. To the best of our knowledge, this is the first example of S_NAr on a transition metal arene complex using exogeneous nucleophiles that does not require a leaving group on the arene nor subsequent oxidation steps. Mechanistic studies show that the reaction involves reversible rear-side addition of the nucleophile followed by an unprecedented intramolecular hydride migration from the metal-stabilised Jackson-Meisenheimer intermediate to the metal centre. This is facilitated by deprotonation of the ^{tBu}PN ligand, which makes the metal centre more electron-rich enabling facile chloride removal and subsequent hydride migration. The versatility of this reaction was shown for a broad variety of diverse nucleophiles, including C_{sp3}, C_{sp2}, C_{sp}, N and P-based nucleophiles. We envision that this new reaction pathway provides the solid foundation for the development of new stoichiometric and catalytic S_NArH reactions.

Methods

General considerations

All manipulations were performed under inert atmosphere using standard Schlenk techniques or inside of a N_2-filled M. Braun glovebox using dry solvents and reagents, unless stated otherwise. Glassware was dried at 130 °C in an oven or with a heat gun under a dynamic vacuum, unless

noted otherwise. Hexane and DCM were collected from an M. Braun MB-SPS-800 solvent purification system and degassed and stored over 4 Å molecular sieves, except for DCM which was dried over 3 Å molecular sieves. THF was dried over Na/benzophenone ketyl (purple), or over Na dispersed on silica spheres, vacuum-transferred and degassed, subsequently followed by storage over 4 Å molecular sieves. Benzene (Scharlab, > 99%) and pentane (technical, VWR chemicals) were degassed, then dried and stored over 4 Å molecular sieves. All non-deuterated solvents were degassed by bubbling N_2 (g) through the solvent for at least 30 min. The solvents (1.0 mL) were tested with a standard purple solution of sodium benzophenone ketyl in THF to confirm effective oxygen and water removal (max 1-2 drops for most solvents, max 4 drops for THF). All solvents were checked for water content by Karl-Fischer titration and all of them were well below 5 ppm. Deuterated solvents were obtained from Cambridge Isotope Laboratories except for THF-d_8, which was obtained from ABCR, degassed by the standard freeze-pump-thaw procedure and stored over 4 Å molecular sieves (3 Å for CD_2Cl_2). All commercial reagents were used as received and were obtained from Sigma Aldrich, Acros and Strem. $^{t\text{Bu}}$PN[44], PhN(SiMe$_3$)$_2$[45], lithium phenylacetylide[46] were prepared according to literature procedures.

NMR measurements

NMR data was recorded on an VNMRS-400 Varian 400 MHz (9.4 T) NMR system equipped with an OneNMR probe (with quartz liner) and Optima Tune system and a Performa IV PFG amplifier capable of generating a 65 G/cm gradient or a Jeol JNM-ECZL G 400 MHz (9.4 T) NMR system equipped with an autotunable ROYALPROBE HFX (with quartz liner) and a gradient amplifier capable of generating a 90 G/cm gradient. All chemical shifts are reported in the standard d notation of parts per million, referenced to the residual solvent peak. All resonances in ^{1}H NMR and ^{13}C NMR spectra were referenced to residual solvent peaks (^{1}H NMR: 7.16 for C_6D_6, 3.58 for THF-d_8, 5.32 for CD_2Cl_2, ^{13}C NMR: 128.06 for C_6D_6, 67.57 for THF-d_8, 53.84 for CD_2Cl_2). The resonances in the ^{31}P NMR spectra are referenced using the absolute reference method from a correctly referenced ^{1}H NMR spectrum of the same sample. The assignment of peaks is based on relative integration, chemical shift, and 2D NMR analysis (COSY, TOCSY, HMBC, HMQC, NOESY, J-resolved experiments). For ^{1}H NMR spectra in non-deuterated solvents, solvent suppression is used (PRESAT). All NMR experiments involving air-sensitive compounds were conducted in J. Young NMR tubes under a N_2 atmosphere. Peak multiplicity was quoted as s (singlet), d (doublet), t (triplet) and so on. For quantitative analyses the acquisition time was chosen so that the full FID was recorded, the relaxation delay was set to 7 times the longest T1, determined by an individual T1 measurement. Inverse gated decoupling was employed where necessary.

Other physical methods

GC analyses were performed on a Perkin-Elmer Clarus 500 Gas Chromatograph equipped with a PE Elite-5 column ((30m x 0.32 mm x 0.25 µm), (5% phenyl)-(95%methyl)polysiloxane) and a flame-ionisation detector. The calculations and plotting of the GC calibration were performed using an in-house script written in the Python programming language (Python Software Foundation. Python Language Reference, version 3.11.4. Available at http://www.python.org). ATR-FTIR spectra were recorded on a PerkinElmer Frontier FTIR spectrometer equipped with a PerkinElmer Universal Attenuated Total Reflectance (ATR) Sampling Accessory with a diamond/ZnSe plate and a LiTaO3 mid-IR detector. IR-analysis of air-sensitive compounds was performed by dropcasting a solution (THF, DCM or pentane) onto the ATR crystal, which was covered by a continues N_2 flow. Elemental analysis was performed by MEDAC Ltd. based in the United Kingdom.

UV experiments

For the UV light irradiation experiments, a set-up was used that consists of a double-walled quartz tube and a UV light source[47]. The UV light source consists of a flexible Waveform Lighting realUVTM 365 nm LED strip lights (2.46 W per 1 metre) wrapped around a brass rod. This type of LED has a single sharp peak at 365 nm in the spectrum. The rod with the LED lights is placed inside the double-walled quartz tube, which is actively cooled with water during irradiation experiments ("cold" UV). When the water cooling is not used ("hot" UV), the quartz tube gets warm (~45 °C). J. Young valved NMR tubes containing the solutions of complexes were then placed around the quartz tube. The standard distance of 1-3 mm between the lamp and an NMR tube was used unless different is stated (see Supplementary Fig. S58).

Synthetic procedures

Note: See Supplementary Section S7 for the spectra of the isolated compounds.

[($^{t\text{Bu}}$PN)RuCl(C_6H_6)][PF_6] (1)

A 100 mL Schlenk tube was charged with $^{t\text{Bu}}$PN (118.7 mg, 0.50 mmol), KPF_6 (115.0 mg, 0.63 mmol) and [$Ru_2Cl_4(C_6H_6)_2$] (125.0 mg, 0.25 mmol). Next, DCM (10.0 mL) was added to give an orange suspension. The reaction mixture was kept stirring in a glovebox at RT for 18 h, the colour of the reaction mixture became dark brown. The mixture was filtered through a glass filter from unreacted KPF_6 and KCl, to give a dark brown filtrate. Volatiles were removed under a dynamic vacuum, the resulting residue was suspended in 3.0 mL of THF and was stirred for 15 min. The mixture was filtered and the residue was dried under a dynamic vacuum giving 132.0 mg (44%) of a bright yellow powder. Crystals suitable for X-ray diffraction analysis were grown by vapor diffusion of THF into a solution of **1** in DCM at room temperature.

*Note: the product has moderate solubility only in DCM and MeCN. Washing with THF (note that as little as possible of THF should be used as **1** is partially soluble in THF) is required to get rid of byproducts of the reaction, the crystal structure of one of them – ($^{t\text{Bu}}$PN)$_2$RuCl$_2$ – was fortuitously also obtained (see Supplementary Section S6.3).*

^{1}H NMR (400 MHz, CD_2Cl_2, 298K): δ = 9.24 (d, $^3J_{H,H}$ = 5.0 Hz, 1H), 7.87 – 7.80 (m, 1H), 7.44 (d, $^3J_{H,H}$ = 7.8 Hz, 1H), 7.39 – 7.34 (m, 1H), 6.11 (d, $^3J_{H,P}$ = 0.7 Hz, 6H), 3.89 (dd, $^2J_{H,H}$ = 16.4, $^2J_{H,P}$ = 8.7 Hz, 1H), 3.31 (dd, $^2J_{H,H}$ = 16.4, $^2J_{H,P}$ = 13.3 Hz, 1H), 1.57 (d, $^3J_{H,P}$ = 14.5 Hz, 9H), 1.21 (d, $^3J_{H,P}$ = 13.4 Hz, 9H).

^{13}C{^{1}H} NMR (101 MHz, CD_2Cl_2, 298K): δ = 163.0 (d, $^4J_{C,P}$ = 3.1 Hz), 157.5 (s), 140.5 (d,), 125.1 (s), 125.0 (s), 89.7 (d, $^2J_{C,P}$ = 2.4 Hz), 39.6 (d, $^1J_{C,P}$ = 2.3 Hz), 39.5 (d, $^2J_{C,P}$ = 3.1 Hz), 33.6 (d, $^1J_{C,P}$ = 23.7 Hz), 31.6 (d, $^2J_{C,P}$ = 2.3 Hz), 29.9 (d, $^2J_{C,P}$ = 2.7 Hz).

^{31}P{^{1}H} NMR (162 MHz, CD_2Cl_2, 298K): δ = 90.8 (s, 1P), –144.4 (hept, $^1J_{P,F}$ = 710.8 Hz, 1P).

^{19}F NMR (376 MHz, CD_2Cl_2, 298K): δ = –72.7 (d, $^1J_{F,P}$ = 711.0 Hz, 6F).

Anal. Calcd. For $C_{20}H_{30}ClNP_2RuF_6$: C, 40.24; H, 5.07; N, 2.35. **Found:** C, 39.69; H, 5.04; N, 2.22.

ATR-IR (film, N_2 flow): ν = 3090 (w), 2964 (m), 2924 (m), 2873 (w), 1607 (w), 1474 (m), 1441 (m), 1387 (w), 1373 (w), 1312 (w), 1269 (w), 1178 (w), 1024 (w), 876 (w), 835 (s), 776 (w), 734 (m), 702 (w), 621 (w), 557 (s), 493 (w), 460 (w) cm^{-1}.

[($^{t\text{Bu}}$PN*)RuCl(C_6H_6)K(THF)$_n$]PF_6 (2-K) and [($^{t\text{Bu}}$PN)RuH(PhN(TMS)$_2$)]PF_6 (3)

A colourless solution of $KN(TMS)_2$ (8.0 mg, 0.04 mmol) in THF-d_8 (1.5 mL) was added dropwise to a yellow suspension of complex **1** (23.9 mg, 0.04 mmol) in THF-d_8 (1.5 mL), resulting in a dark brown solution. The vial with the reaction mixture was kept stirring for 15 min at RT after which a sample was transferred into a J. Young tube and analysed by NMR spectroscopy.

*Note: the crude ^{1}H NMR spectrum shows the formation of ~50% species **2-K** and ~20% species **3** based on the relative integral values. For a cleaner synthesis route towards **2-K** as well as an alternative route to the mixture of **2K** and **3** see Supplementary Section S1.2.*

For **2-K**:

^{1}H NMR (400 MHz, THF-d_8, 298 K): δ = 8.21 (ddd, J = 5.3, 1.6, 1.2 Hz, 1H), 7.62 (ddd, J = 7.9, 7.9, 1.5 Hz, 1H), 7.06 (dddd, J = 7.8, 5.3, 1.3, 1.3 Hz, 1H), 6.72 (dd, J = 7.9, 1.0 Hz, 1H), 5.82 (s, 6H), 3.33 (d, $^2J_{H,P}$ = 3.0 Hz, 1H), 1.36 (d, $^3J_{H,P}$ = 14.9 Hz, 9H), 1.08 (d, $^3J_{H,P}$ = 15.4 Hz, 9H).

^{31}P{^{1}H} NMR (162 MHz, THF-d_8, 298K): δ = 97.5 (s, 1P), –144.5 (hept, $^1J_{P,F}$ = 710.1 Hz, 1P).

For **3**:

^{1}H NMR (400 MHz, THF-d_8, 298 K): δ = 8.86 (d, J = 5.4 Hz, 1H), 7.71 (t, J = 8.3 Hz, 1H), 7.51 (d, J = 7.6 Hz, 1H), 7.14 (dd, J = 7.6, 6.7 Hz, 1H), 6.27 (t, J = 6.2 Hz, 1H), 6.21 (d, J = 5.5 Hz, 1H), 5.69 (dd, J = 6.2, 1.5 Hz, 1H), 5.44 – 5.39 (m, 1H), 4.64 (dt, J = 5.9, 1.6 Hz, 1H), 3.64 – 3.56 (m, 1H, overlapped with a THF signal), 3.26 (dd, J = 17.2, 7.6 Hz, 1H), 1.34 (d, $^3J_{H,P}$ = 13.7 Hz, 9H), 1.25 (d, $^3J_{H,P}$ = 13.0 Hz, 9H), 0.30 (s, 18H), –7.77 (d, J = 42.5 Hz, 1H).

^{31}P{^{1}H} NMR (162 MHz, THF-d_8, 298K): δ = 111.8 (d*, $^2J_{P,H}$ = 11.2 Hz, 1P), –144.5 (hept, $^1J_{P,F}$ = 710.1 Hz, 1P).

**The doublet appears due to partial coupling with the hydride.*

($^{t\text{Bu}}$PN*)RuH(PhN(TMS)$_2$) (4)

A yellow suspension of complex **1** (96.8 mg, 0.16 mmol) in 6.0 mL of THF was added dropwise to a colourless solution of $KN(TMS)_2$ (64.7 mg, 0.32 mmol) in 4.0 mL of THF. The starting complex instantly dissolved upon the addition resulting in a colour change to dark brown. The vial with the reaction mixture was kept stirring for 0.5 h at RT. The mixture was dried under a dynamic vacuum to give a dark brown solid. The residue was extracted with pentane (5.0 mL), and the extracts were dried under a dynamic vacuum to give a dark brown sticky solid (90.3 mg, 97%). Crystals suitable for X-ray diffraction analysis were grown by keeping a concentrated solution of **4** in pentane at –40 °C.

^{1}H NMR (400 MHz, C_6D_6, 298 K): δ = 7.33 (dd, $^3J_{H,H}$ = 6.3, $^4J_{H,H}$ = 0.9 Hz, 1H), 6.53 (dddd, $^3J_{H,H}$ = 9.0, $^3J_{H,H}$ = 6.3, $^5J_{H,P}$ = 2.1, $^4J_{H,H}$ = 1.4 Hz, 1H), 6.41 (d, $^3J_{H,H}$ = 8.8 Hz, 1H), 5.38 (ddd, $^3J_{H,H}$ = 7.1, $^3J_{H,H}$ = 6.3, $^4J_{H,H}$ = 1.4 Hz, 1H), 5.11 (dd, $^3J_{H,H}$ = 6.2, $^3J_{H,H}$ = 5.9 Hz, 1H), 4.94 (dd, $^3J_{H,H}$ = 6.2, $^3J_{H,H}$ = 5.2 Hz, 1H), 4.77 (dd, $^3J_{H,H}$ = 6.0, $^3J_{H,H}$ = 4.9 Hz, 1H), 4.67 (dd, $^3J_{H,H}$ = 6.0, $^3J_{H,H}$ = 1.9 Hz, 1H), 4.14 (ddd, $^3J_{H,H}$ = 5.7, $^4J_{H,H}$ = 2.2, $^4J_{H,H}$ = 1.8 Hz, 1H), 3.49 (d, $^2J_{H,P}$ = 2.6 Hz, 1H), 1.31 (d, $^3J_{H,P}$ = 12.4 Hz, 9H), 1.27 (d, $^3J_{H,P}$ = 13.2 Hz, 9H), 0.25 (s, 18H), –7.76 (d, $^2J_{H,P}$ = 43.4 Hz, 1H).

^{13}C{^{1}H} NMR (101 MHz, C_6D_6, 298 K) δ = 170.9 (d, $^2J_{C,P}$ = 15.6 Hz), 154.4 (s), 130.8 (d, $^4J_{C,P}$ = 2.3 Hz), 130.7 (s), 115.2 (d, $^3J_{C,P}$ = 17.2 Hz), 101.4 (s), 92.4 (s), 90.6 (d, $^2J_{C,P}$ = 5.7 Hz), 83.4 (s),

77.4 (s), 74.1 (d, $^{2}J_{C,P}$ = 3.1 Hz), 62.3 (d, $^{1}J_{C,P}$ = 60.3 Hz), 38.3 (d, $^{1}J_{C,P}$ = 14.5 Hz), 36.2 (d, $^{1}J_{C,P}$ = 34.3 Hz), 31.1 (d, $^{2}J_{C,P}$ = 3.4 Hz), 30.2 (d, $^{2}J_{C,P}$ = 5.0 Hz), 3.3 (s).

$^{31}P\{^{1}H\}$ NMR (162 MHz, C_6D_6, 298 K): δ = 98.8 (s).

ATR-IR (film, N_2 flow): ν = 3045 (m), 2954 (s), 2864 (s), 2893 (m), 2034 (w, br), 1604 (s), 1535 (w), 1511 (w), 1488 (s), 1446 (s), 1381 (w), 1359 (w), 1358 (w), 1285 (m), 1253 (m), 1225 (m), 1205 (m), 1179 (w), 1146 (w), 1101 (w), 1017 (w), 1000 (m), 933 (m), 892 (s), 840 (m), 810 (m), 758 (w), 726 (w), 687 (w), 667 (w), 616 (w), 503 (w), 463 (w) cm^{-1}.

*Despite several attempts using spectroscopically pure samples, the reactive nature of **4** precluded obtaining a satisfactory elemental analysis.*

*X-ray crystal structure determination of **4***

$C_{26}H_{47}N_2PRuSi_2$, Fw = 575.87, orange block, 0.41 × 0.40 × 0.17 mm^3, monoclinic, $P2_1/c$ (no. 14), a = 13.9298(4), b = 16.2626(4), c = 13.8275(4) Å, β = 112.534(2) , V = 2893.25(15) $Å^3$, Z = 4, D_x = 1.322 g/cm^3, μ = 0.70 mm^{-1}. The diffraction experiment was performed on a Bruker Kappa ApexII diffractometer with sealed tube and Triumph monochromator (λ = 0.71073 Å) at a temperature of 150(2) K up to a resolution of $(\sin\theta/\lambda)_{max}$ = 0.65 $Å^{-1}$. The crystal was broken into several fragments. Two orientation matrices were used for the intensity integration of the major fragments using the Eval15 software[48]. Only the non-overlapping reflections were used for structure solution and refinement. A multi-scan absorption correction and scaling was performed with SADABS[49] (correction range 0.68-0.75). A total of 41381 reflections was measured, 6635 reflections were unique (R_{int} = 0.021), 6179 reflections were observed [I>2σ(I)]. The structure was solved with Patterson superposition methods using SHELXT.[50] Structure refinement was performed with SHELXL-2018[51] on F^2 of all reflections. Non-hydrogen atoms were refined freely with anisotropic displacement parameters. All hydrogen atoms were located in difference Fourier maps. Metal-bound hydrogen atom H1 and hydrogens H16-H20 of the coordinated phenyl group were refined freely with isotropic displacement parameters. All other hydrogen atoms were refined with a riding model. 329 Parameters were refined with no restraints. R1/wR2 [I > 2σ(I)]: 0.0200 / 0.0507. R1/wR2 [all refl.]: 0.0217 / 0.0516. S = 1.045. Residual electron density between –0.42 and 0.49 e/$Å^3$. Geometry calculations and checking for higher symmetry was performed with the PLATON program.[52]

For structural details see Supplementary Section S6.2.

Computational details

All calculations were carried out using DFT[53] as implemented in ORCA 5.0.3.[54–56] Geometry optimisations were performed with the B3LYP[57,58] including Grimme's D3 dispersion correction with Becke-Johnson Damping.[55–63] Geometry optimisations and analytical vibrational frequency calculations were carried out with the def2-SVP basis set[65] with def2-ECP for Ru.[64] For all optimised structures, the intermediates were confirmed with no imaginary vibrational frequency, while transition states showed a single imaginary frequency with a motion corresponding to the proper transitions. The solvated energies of optimised structures were re-evaluated by additional single-point calculations on each optimised geometry using the def2-TZVPP basis set.[65] For all calculations, the RIJCOSX approximation[66,67] was utilised with the auxiliary basis set def2/J.[68] To

model the solution environment for tetrahydrofuran, the solvation model based on density (SMD)[69] was utilised with parameters which have been implemented in ORCA. TD-DFT[70] calculations for modelling excited states were conducted as implemented in Q-Chem 5.4 software.[71] Geometries from the optimised geometry with ORCA were utilised for the calculations of excited states. Single Excitation Configuration Interaction (CIS)[72] and Tamm-Dancoff approximation were utilised to reduce the computation cost without damage to the quality of the results. The functional and basis set for the calculations of the excited state are identical to those for DFT calculations.

Data availability

All data can be found in the main text, Methods section or the Supplementary Materials. CCDC 2355856-2355858 contain the supplementary crystallographic data for this paper. These data can be obtained free of charge from The Cambridge Crystallographic Data Centre via www.ccdc.cam.ac.uk/data_request/cif. The spectroscopic files that support the findings of this study are openly available in the Yoda data repository at DOI: https://doi.org/10.24416/UU01-BYOFTG.

Acknowledgements

This research was funded in part by The Netherlands Organization for Scientific Research (Grant OCENW.M20.016 to D. L. J. B). We thank the Institute for Basic Science in Korea for financial support (IBS-R010-A1). The X-ray diffractometer has been financed by the Netherlands Organization for Scientific Research (NWO). We deeply thank Dr. M.-E. Moret, Dr. S. Tretiakov, E. Kounalis, R. Bienenmann, L. Killian and L. Riddell for fruitful discussions and suggestions throughout the project.

Author contributions

S.M. and D.L.J.B. conceived the project. S.M. performed the experiments including the synthesis, characterisation and analysis. D.H. and B.P. carried out computational calculations. M.L. performed crystallographic measurements including the acquisition, solving and interpretation of the crystal structures. D.L.J.B. supervised the project. The original draft was written by S.M. and was reviewed by M.-H.B. and D.L.J.B. with contributions by all authors.

Ethics declaration

The authors declare no conflict of interests.

References

1. C. Friedel, J.-M. Crafts. Sur une nouvelle méthode générale de synthèse hydrocarbures, d'acétones, etc. *Compt. Rend.* **84**, (1877).
2. Ashdown, A. A. Earliest History of the Friedel-Crafts Reaction. *Ind. Eng. Chem.* **19**, 1063–1065 (1927).
3. Mąkosza, M. Electrophilic and nucleophilic aromatic substitution: Analogous and complementary processes. *Russ. Chem. Bull.* **45**, 491–504 (1996).
4. Mąkosza, M. Electrophilic and Nucleophilic Aromatic Substitutions are Mechanistically Similar with Opposite Polarity. *Chem. – Eur. J.* **26**, 15346–15353 (2020).
5. Terrier, F. *Modern Nucleophilic Aromatic Substitution*. (John Wiley & Sons, 2013).
6. Błaziak, K., Danikiewicz, W. & Mąkosza, M. How Does Nucleophilic Aromatic Substitution Really Proceed in Nitroarenes? Computational Prediction and Experimental Verification. *J. Am. Chem. Soc.* **138**, 7276–7281 (2016).
7. Artamkina, G. A., Egorov, M. P. & Beletskaya, I. P. Some aspects of anionic σ-complexes. *Chem. Rev.* **82**, 427–459 (1982).
8. Mąkosza, M. & Kwast, A. Vicarious nucleophilic substitution of hydrogen. Mechanism and orientation. *J. Phys. Org. Chem.* **11**, 341–349 (1998).
9. Mąkosza, M. Nucleophilic substitution of hydrogen in electron-deficient arenes, a general process of great practical value. *Chem. Soc. Rev.* **39**, 2855–2868 (2010).
10. Card, R. J. & Trahanovsky, W. S. Arene-metal complexes. 12. Reaction of (η^6-benzene)tricarbonylchromium with *n*-butyllithium. *J. Org. Chem.* **45**, 2555–2559 (1980).
11. Rose-Munch, F. & Rose, E. cine and tele Nucleophilic Substitutions in (η^6-Arene)tricarbonylchromium and Tricarbonyl(η^5-cyclohexadienyl)manganese Complexes. *Eur. J. Inorg. Chem.* **2002**, 1269–1283 (2002).
12. Semmelhack, M. F. *et al.* Addition of carbon nucleophiles to arene-chromium complexes. *Tetrahedron* **37**, 3957–3965 (1981).
13. Pigge, F. & Coniglio, J. J. Stoichiometric applications of η^6-Arene Ruthenium (II) complexes in organic chemistry. *Curr. Org. Chem.* **5**, 757–784 (2001).
14. Werner, H., Werner, R. & Burschka, C. Aromaten(phosphan)metall-Komplexe, V. Zur Addition von Carbanionen an (Benzol)ruthenium(II)- und -osmium(II)-Komplexe. Kristall- und Molekülstruktur von (*exo*-6-*n*-C_4H_9-η^5-C_6H_6)OsI(PMe_3)$_2$. *Chem. Ber.* **117**, 152–160 (1984).
15. Boone, M. P. & Stephan, D. W. Ru-η^6-Arene Cations [($Ph_2PC_6H_4$)$_2$B(η^6-Ph)RuX]$^+$ (X=Cl, H) as Lewis Acids. *Chem. – Eur. J.* **20**, 3333–3341 (2014).
16. Ponikiewski, Ł. *et al.* Reactions of the Lithiated Diphosphine ^{t}Bu$_2$P–P($SiMe_3$)Li with [(η^6-C_6H_6)$RuCl_2$]$_2$ in the Presence of Tertiary Phosphines. *Eur. J. Inorg. Chem.* **2016**, 4241–4249 (2016).
17. Munro, G. A. M. & Pauson, P. L. Alkyl and Acyl Dicarbonylarenemanganese Complexes: The Reduction of Metal-Bound Carbonyl Groups. *Isr. J. Chem.* **15**, 258–261 (1976).
18. Brookhart, M., Pinhas, A. R. & Lukacs, A. Reaction of lithium dimethylcuprate with $C_6H_6Mn(CO)_3^+$. Observation of methyl group migration from manganese to the arene ring in $C_6H_6(CO)_2MnMe$. *Organometallics* **1**, 1730–1731 (1982).
19. Semmelhack, M. F. *et al.* η^5-Cyclohexadienyltricarbonylchromium(0) complexes from addition of carbon nucleophiles to η^6-benzenetricarbonylchromium(0). Formation, chemical and spectroscopic features, and x-ray diffraction analysis. *J. Am. Chem. Soc.* **101**, 3535–3544 (1979).
20. Davies, S. G., Green, M. L. H. & Mingos, D. M. P. Nucleophilic addition to organotransition metal cations containing unsaturated hydrocarbon ligands: A survey and interpretation. *Tetrahedron* **34**, 3047–3077 (1978).
21. Winkhaus, G., Pratt, L. & Wilkinson, G. 738. π-Cyclohexadienylmanganese tricarbonyl and related compounds. *J. Chem. Soc. Resumed* **0**, 3807–3813 (1961).

22. Pearson, A. J. & Heo, J.-N. Approaches to the Fully Functionalized DEF Ring System of Ristocetin A via Highly Selective Ruthenium-Promoted S_NAr Reaction. *Org. Lett.* **2**, 2987–2990 (2000).
23. Chen, K., Ma, Y., Lin, Y., Li, J.-Y. & Shi, H. Ruthenium/η^5-Phenoxo-Catalyzed Amination of Phenols with Amines. *J. Am. Chem. Soc.* **146**, 15833–15842 (2024).
24. Schulte, T. *et al.* Ruthenium Phenoxo Complexes: An Isolobal Ligand to Cp with Improved Properties. *J. Am. Chem. Soc.* **146**, 15825–15832 (2024).
25. D'Amato, E. M., Neumann, C. N. & Ritter, T. Selective Aromatic C–H Hydroxylation Enabled by η^6-Coordination to Iridium(III). *Organometallics* **34**, 4626–4631 (2015).
26. Eloi, A. *et al.* Cationic Planar Chiral (η^6-Arene)$Mn(CO)_3^+$ Complexes: Resolution, NMR Study in Chiral-Oriented Solvents, and Applications to the Enantioselective Synthesis of 4-Substituted Cyclohexenones and (η^6-Phosphinoarene)$Mn(CO)_3^+$ Complexes. *Organometallics* **29**, 3876–3886 (2010).
27. Semmelhack, M. F. & Clark, G. Meta-substituted aromatics by carbanion attack on π-anisole and π-toluenechromium tricarbonyl. *J. Am. Chem. Soc.* **99**, 1675–1676 (1977).
28. Cambie, R. C. *et al.* Recations of cationic (η^6-chloroarene) complexes of iron and ruthenium with some O-silyl and C-silyl compounds. *J. Organomet. Chem.* **409**, 385–409 (1991).
29. Wilson, A. S., Hill, M. S., Mahon, M. F., Dinoi, C. & Maron, L. Organocalcium-mediated nucleophilic alkylation of benzene. *Science* **358**, 1168–1171 (2017).
30. Rösch, B. *et al.* Nucleophilic aromatic substitution at benzene with powerful strontium hydride and alkyl complexes. *Angew. Chem.* **131**, 5450–5455 (2019).
31. Richardson, G. M. *et al.* Hydroarylation of olefins catalysed by a dimeric ytterbium (II) alkyl. *Nat. Commun.* **12**, 1–7 (2021).
32. Qu, Z.-W., Zhu, H., Streubel, R. & Grimme, S. Organo-Group 2 Metal-Mediated Nucleophilic Alkylation of Benzene: Crucial Role of Strong Cation-π Interaction. *ACS Catal.* **13**, 1686–1692 (2023).
33. Khusnutdinova, J. R. & Milstein, D. Metal–Ligand Cooperation. *Angew. Chem. Int. Ed.* **54**, 12236–12273 (2015).
34. Groom, C. R., Bruno, I. J., Lightfoot, M. P. & Ward, S. C. The Cambridge Structural Database. *Acta Crystallogr. Sect. B Struct. Sci. Cryst. Eng. Mater.* **72**, 171–179 (2016).
35. Arquier, D. *et al.* Crucial Role of the Amidine Moiety in Methylenamino Phosphine-Type Ligands for the Synthesis of Tethered η^6-Arene- η^1-P Ruthenium(II) Complexes: Experimental and Theoretical Studies. *Organometallics* **28**, 4945–4957 (2009).
36. Bennett, M. A., Robertson, G. B. & Smith, A. K. Divalent ruthenium complexes containing non-planar *hexahapto*-benzene. *J. Organomet. Chem.* **43**, C41–C43 (1972).
37. Burrows, J., Kamo, S. & Koide, K. Scalable Birch reduction with lithium and ethylenediamine in tetrahydrofuran. *Science* **374**, 741–746 (2021).
38. Schwartsburd, L., Iron, M. A., Konstantinovski, L., Ben-Ari, E. & Milstein, D. A Dearomatized Anionic PNP Pincer Rhodium Complex: C–H and H–H Bond Activation by Metal–Ligand Cooperation and Inhibition by Dinitrogen. *Organometallics* **30**, 2721–2729 (2011).
39. Ben-Ari, E., Leitus, G., Shimon, L. J. W. & Milstein, D. Metal−Ligand Cooperation in C−H and H_2 Activation by an Electron-Rich PNP Ir(I) System: Facile Ligand Dearomatization−Aromatization as Key Steps. *J. Am. Chem. Soc.* **128**, 15390–15391 (2006).
40. Spivey, J. A. & Collum, D. B. Potassium Hexamethyldisilazide (KHMDS): Solvent-Dependent Solution Structures. *J. Am. Chem. Soc.* (2024) doi:10.1021/jacs.4c03418.
41. Shvydkiy, N. V. & Perekalin, D. S. Reactions of arene replacement in transition metal complexes. *Coord. Chem. Rev.* **411**, 213238 (2020).
42. Choi, M.-G., Ho, T. C. & Angelici, R. J. Arene Binding Affinities in [CpRu(η^6-arene)]$^+$ Complexes: Models for the Adsorption of Arenes on Hydrodesulfurization Catalysts. *Organometallics* **27**, 1098–1105 (2008).

43. Olaj, O. F., Kauffmann, H. F. & Breitenbach, J. W. The Diels-Alder intermediate as a chain transfer agent in spontaneous styrene polymerization 1. New evidence from the kinetic analysis of photoinitiated polymerization. *Makromol. Chem.* **177**, 3065–3071 (1976).
44. Fanara, P. M., MacMillan, S. N. & Lacy, D. C. Planar-Locked Ru-PNN Catalysts in 1-Phenylethanol Dehydrogenation. *Organometallics* **39**, 3628–3644 (2020).
45. Keck, C., Maichle-Mössmer, C. & Bettinger, H. F. Photo electron transfer induced desilylation of N,N-bis(trimethylsilyl)aminodibenzoborole to aminodibenzoborole. *Chem. Commun.* **55**, 7470–7473 (2019).
46. Wang, Y., Zhang, W.-X., Wang, Z. & Xi, Z. Procedure-Controlled Selective Synthesis of 5-Acyl-2-iminothiazolines and their Selenium and Tellurium Derivatives by Convergent Tandem Annulation. *Angew. Chem. Int. Ed.* **50**, 8122–8126 (2011).
47. Beek, C. B. van *et al.* Combining metal–metal cooperativity, metal–ligand cooperativity and chemical non-innocence in diiron carbonyl complexes. *Chem. Sci.* **13**, 2094–2104 (2022).
48. Schreurs, A. M., Xian, X. & Kroon-Batenburg, L. M. EVAL15: a diffraction data integration method based on ab initio predicted profiles. *J. Appl. Crystallogr.* **43**, 70–82 (2010).
49. Krause, L., Herbst-Irmer, R., Sheldrick, G. M. & Stalke, D. Comparison of silver and molybdenum microfocus X-ray sources for single-crystal structure determination. *J. Appl. Crystallogr.* **48**, 3–10 (2015).
50. Sheldrick, G. M. SHELXT–Integrated space-group and crystal-structure determination. *Acta Crystallogr. Sect. Found. Adv.* **71**, 3–8 (2015).
51. Sheldrick, G. M. Crystal structure refinement with SHELXL. *Acta Crystallogr. Sect. C Struct. Chem.* **71**, 3–8 (2015).
52. Spek, A. L. Structure validation in chemical crystallography. *Acta Crystallogr. D Biol. Crystallogr.* **65**, 148–155 (2009).
53. Parr, R. G. & Weitao, Y. *Density-Functional Theory of Atoms and Molecules*. (Oxford University Press, 1994).
54. Neese, F. The ORCA program system. *WIREs Comput. Mol. Sci.* **2**, 73–78 (2012).
55. Neese, F. Software update: the ORCA program system, version 4.0. *WIREs Comput. Mol. Sci.* **8**, e1327 (2018).
56. Neese, F. Software update: The ORCA program system—Version 5.0. *WIREs Comput. Mol. Sci.* **12**, e1606 (2022).
57. Becke, A. D. A new mixing of Hartree–Fock and local density-functional theories. *J. Chem. Phys.* **98**, 1372–1377 (1993).
58. Lee, C., Yang, W. & Parr, R. G. Development of the Colle-Salvetti correlation-energy formula into a functional of the electron density. *Phys. Rev. B Condens. Matter* **37**, 785–789 (1988).
59. Grimme, S., Antony, J., Ehrlich, S. & Krieg, H. A consistent and accurate *ab initio* parametrization of density functional dispersion correction (DFT-D) for the 94 elements H-Pu. *J. Chem. Phys.* **132**, 154104 (2010).
60. Grimme, S., Ehrlich, S. & Goerigk, L. Effect of the damping function in dispersion corrected density functional theory. *J. Comput. Chem.* **32**, 1456–1465 (2011).
61. Slater, J. C. & Phillips, J. C. Quantum Theory of Molecules and Solids Vol. 4: The Self-Consistent Field for Molecules and Solids. *Phys. Today* **27**, 49–50 (1974).
62. Vosko, S. H., Wilk, L. & Nusair, M. Accurate spin-dependent electron liquid correlation energies for local spin density calculations: a critical analysis. *Can. J. Phys.* **58**, 1200–1211 (1980).
63. Becke, A. D. Density-functional exchange-energy approximation with correct asymptotic behavior. *Phys. Rev. A* **38**, 3098–3100 (1988).
64. Becke, A. D. Density-functional thermochemistry. III. The role of exact exchange. *J. Chem. Phys.* **98**, 5648–5652 (1993).
65. Weigend, F. & Ahlrichs, R. Balanced basis sets of split valence, triple zeta valence and quadruple zeta valence quality for H to Rn: Design and assessment of accuracy. *Phys. Chem. Chem. Phys.* **7**, 3297–3305 (2005).

66. Andrae, D., Häußermann, U., Dolg, M., Stoll, H. & Preuß, H. Energy-adjusted *ab initio* pseudopotentials for the second and third row transition elements. *Theor. Chim. Acta* **77**, 123–141 (1990).
67. Neese, F. An improvement of the resolution of the identity approximation for the formation of the Coulomb matrix. *J. Comput. Chem.* **24**, 1740–1747 (2003).
68. Helmich-Paris, B., De Souza, B., Neese, F. & Izsák, R. An improved chain of spheres for exchange algorithm. *J. Chem. Phys.* **155**, 104109 (2021).
69. Weigend, F. Accurate Coulomb-fitting basis sets for H to Rn. *Phys. Chem. Chem. Phys.* **8**, 1057–1065 (2006).
70. Marenich, A. V., Cramer, C. J. & Truhlar, D. G. Universal Solvation Model Based on Solute Electron Density and on a Continuum Model of the Solvent Defined by the Bulk Dielectric Constant and Atomic Surface Tensions. *J. Phys. Chem. B* **113**, 6378–6396 (2009).